THE JOURNAL OF PHYSICAL CHEMISTRY LETTERS
A JOURNAL OF THE AMERICAN CHEMICAL SOCIETY

pubs.acs.org/JPCL
Letter

High-Valent Intermediate Observed in a Cu-Based OER Electrocatalyst by *Operando* X-ray Absorption Spectroscopy

Raul Garcia-Diez,* Romualdus Enggar Wibowo, Elmar Kataev, Wilson Quevedo Garzon, Marianne van der Merwe, Daniel Duarte-Ruiz, Caterina Cocchi, and Marcus Bär

Cite This: *J. Phys. Chem. Lett.* 2025, 16, 6328−6333
Read Online

ABSTRACT: Understanding the chemical transformations governing the oxygen evolution reaction (OER) in Cu-based electrocatalysts is critical for advancing cost-efficient alkaline water-splitting technologies. In this study, we employ synchrotron-based *operando* Cu L_3-edge X-ray absorption spectroscopy (XAS) and potentiodynamic techniques to probe the key intermediate species involved in alkaline OER. Our findings reveal that this metastable species exhibits an electronic structure resembling high-valent Cu complexes, particularly those associated with the CuO_2^- ion. Potentiodynamic measurements indicate that the high-valent intermediate emerges at potentials as low as 1.62 V_{RHE}, coinciding with the oxidative process traditionally attributed to the $Cu^{2+} \leftrightarrow Cu^{3+}$ redox transition, suggesting that the formation of the high-valent intermediate is directly linked to this redox process. This work provides valuable insights into the interplay between redox chemistry and catalytic performance in Cu-based OER electrocatalysts and provides further insights into the nature of the chemical species governing the oxygen evolution reaction mechanism.

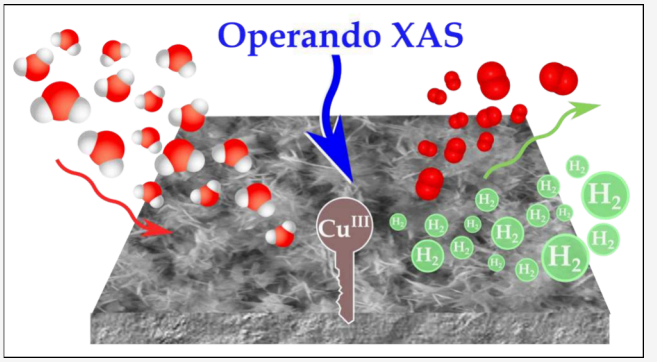

As the global push for decarbonization intensifies, the production of green hydrogen through water electrolysis has emerged as a pivotal technology for achieving clean and sustainable energy systems. Due to the sluggish kinetics of the oxygen evolution reaction (OER), the search for efficient and cost-effective OER electrocatalysts has generated significant research interest. Although precious metal-based materials, such as Ir and Ru oxides, remain the state-of-the-art OER catalysts,[1] the need for cost reduction and scalability has driven the exploration of earth-abundant alternatives such as 3d transition metals. Among these, copper-containing catalysts have emerged as promising candidates in alkaline media,[2,3] including CuO-based materials with OER activities[4,5] comparable to more renowned approaches containing nickel or cobalt,[6,7] which are, however, considered to be critical elements by the US Geological Survey.[8] Hence, a deeper understanding of the reaction mechanism in copper-based electrocatalysts is essential for the knowledge-driven design of materials with enhanced OER activity and for developing strategies to mitigate their severe instability in high alkaline conditions, such as transpassive dissolution[9] or corrosion.[10,11]

Intermediate species play a critical role in the OER pathways, and their identification during operation is crucial for understanding the active phase of copper-based electrocatalysts in alkaline media and the reasons underlying the catalyst's degradation. High-valent Cu complexes are frequently identified as key intermediates in oxidative electrochemical reactions like glucose electrooxidation in nonenzymatic glucose sensors[12,13] or OER. $Cu^{III}{}_2O_3$, originally described by Müller,[14] and $Cu^{III}OOH$,[15] in analogy with $Ni^{III}OOH$, have been proposed as OER intermediates, with the former being recently suggested to decompose into $Cu^{II}O$ through oxygen release.[2] Raman spectroscopic studies by Deng et al.[16] under relevant operation conditions identified a $Cu^{III}O_2^-$ species with a similar fingerprint to $NaCu^{III}O_2$, whereas Ostervold et al.[17] highlighted hydroxide adsorption on the $Cu^{II}O$ surface ($CuO\text{-}(OH^*)_{1/2}$) as the critical intermediate. In contrast, Toparli et al.[9] identified Cu_4O_3 as the most likely intermediate for the OER and subsequent transpassive dissolution. Complementarily, several calculated Pourbaix diagrams[18−20] suggest the formation of a solvated hydroxide species, $Cu^{II}(OH)_4^{2-}$, under these conditions. Conclusive elucidation of the reaction pathways of alkaline OER in copper-based electrocatalysts is still missing, and despite a broad consensus about the participation of a high-valent Cu complex, no element-specific direct method was used to probe

Received: March 28, 2025
Revised: May 21, 2025
Accepted: June 5, 2025
Published: June 14, 2025

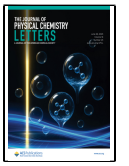

https://doi.org/10.1021/acs.jpclett.5c00944
J. Phys. Chem. Lett. 2025, 16, 6328−6333

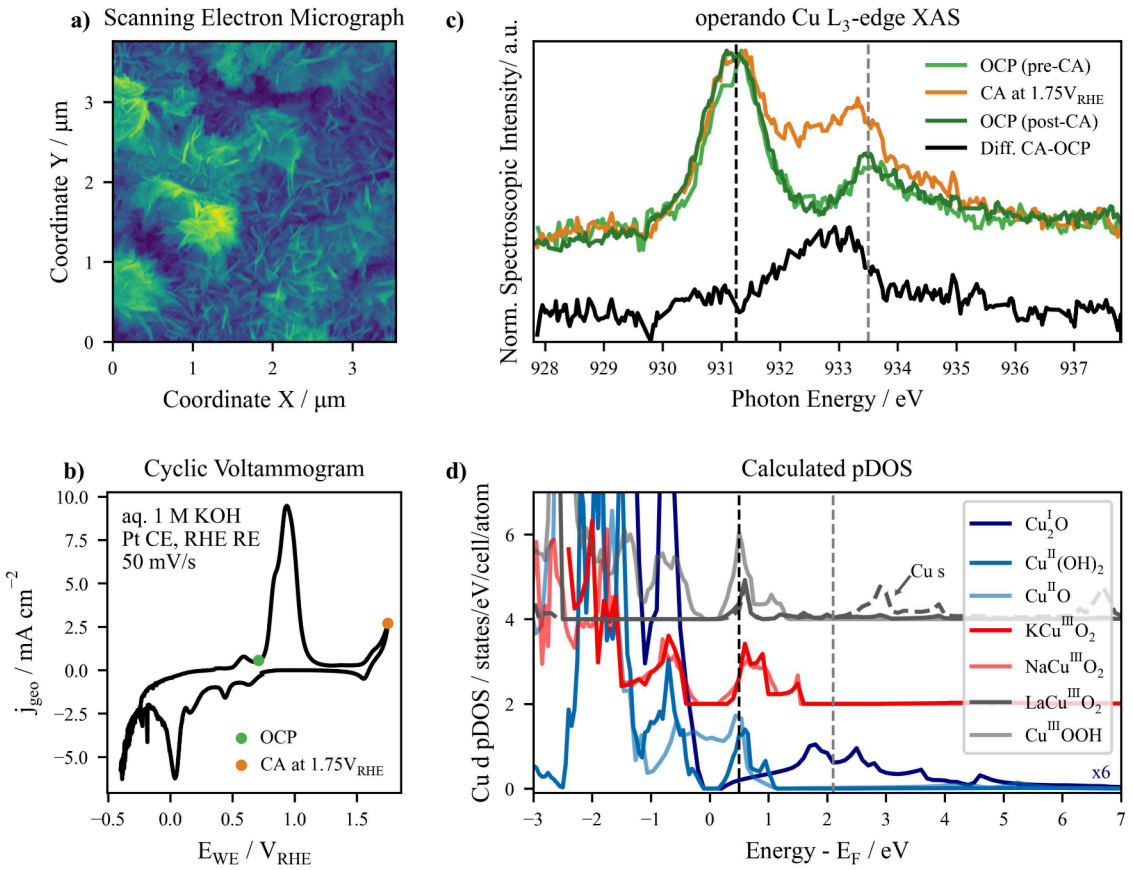

Figure 1. Characterization of the high surface area Cu-based electrocatalyst and speciation of the OER intermediate: (a) Scanning Electron Micrograph (SEM) of the catalyst. (b) Cyclic voltammogram (CV) of the catalyst in aq. 1 M KOH with a scan rate of 50 mV/s. (c) Normalized *operando* Cu L_3-edge XAS of the catalyst under OER conditions (chronoamperometry (CA) at 1.75 V_{RHE}) and at open circuit potential (OCP) before and after CA. The difference between the spectra measured at OCP (pre-CA, dark blue line) and during the CA at OER (red line) is shown below (black line). The (reversible) appearance of a peak around 932.6 eV only under applied potential above the OER onset hints at the formation of the sought-after OER intermediate. The vertical dashed lines indicate the peak energy of Cu^I and Cu^{II} oxides. (d) Calculated Cu d-states: Projected density of states (pDOS) calculated from DFT of complexes related to the electrocatalyst species at OCP (in blue, $Cu^{II}(OH)_2$, $Cu^{II}O$, and Cu^{I}_2O multiplied by 6), of complexes potentially related to the OER intermediate species ($KCu^{III}O_2$ and $NaCu^{III}O_2$ in red), and of other high-valent Cu complexes ($LaCu^{III}O_2$ and $Cu^{III}OOH$ in gray). The Cu s-states of $LaCu^{III}O_2$ are shown for completeness. The vertical dashed lines indicate the LUMO energy of Cu^I and Cu^{II} oxides.

the electronic structure of the intermediate under operating conditions and link it to the calculated structure.

To resolve these ambiguities, *operando* X-ray absorption spectroscopy (XAS) emerges as an ideal tool[21] for probing intermediates that may otherwise evade detection due to their short lifetimes. The accumulation of an intermediate within the time scale accessible by *operando* methods requires that the OER intermediate stabilizes kinetically on the surface of the catalyst and becomes dominant, typically associated with the species at the rate-determining step in the mechanism pathway.[22] In particular, XAS at the Cu $L_{2,3}$-edge provides exceptional chemical sensitivity and insights into electronic transitions involving the active 3d-states.[23] Synchrotron-based *operando* Cu $L_{2,3}$-edge XAS is uniquely suited to capture the electronic configuration of Cu-based species under realistic electrochemical conditions with reasonable time resolution[24] and can provide a deeper understanding of the hybridization of Cu 3d- and O 2p-states,[25] which likely dictates the catalytic activity.

In this study, we employed *operando* Cu L_3-edge XAS on a high surface area copper-based electrocatalyst under applied potentials relevant to alkaline OER to probe the elusive high-valent Cu intermediates. Prepared by the electrochemical anodizing process[26] described in Materials and Experimental Methods in the Supporting Information, the investigated electrocatalyst presents a high surface-to-bulk ratio, as shown in the Scanning Electron Micrograph in Figure 1a. A high surface area is essential to maximize the spectroscopic signal from the electrochemically active species, considering that the measured signal is a convolution of the surface's contribution and the inactive bulk-originated one, due to the large attenuation length of X-rays at the Cu L_3-edge (around 80 nm for metallic copper).

The studied electrocatalyst presents the characteristic cyclic voltammogram (CV) of copper in an alkaline medium, as depicted in Figure 1b for a measurement in aqueous 1 M KOH using the *operando* flow-through cell described by Garcia-Diez et al.[27] CVs show a slight dependence on the sample's history and the solution's molarity, but the overall shape remains consistent. Below 1.3 V_{RHE}, the 1 M KOH CV shows the redox peaks typically ascribed in its anodic branch to subsequent superficial oxidations of Cu to Cu^I_2O and to $Cu^{II}(OH)_2$ or $Cu^{II}O$.[28,29] Interestingly, a redox couple around 1.62 V_{RHE} in the forward cycling direction and 1.55 V_{RHE} in the reverse scan appears just below the potentials relevant for water oxidation operation. Although extensively attributed to the $Cu^{2+} \leftrightarrow Cu^{3+}$

https://doi.org/10.1021/acs.jpclett.5c00944
J. Phys. Chem. Lett. 2025, 16, 6328−6333

reaction,[30−32] accurate identification of this redox process is essential for understanding the chemical transformations occurring during the OER regime. The potential of this Cu redox formation coincides with the onset of the OER-relevant potential regime; therefore, these *operando* investigations were made focusing on potentials in this region and above.

To understand the chemical transformation of the Cu-based electrocatalyst due to oxygen evolution, synchrotron-based Cu L_3-edge absorption spectra are measured in the OÆSE endstation[27] at the EMIL beamline in BESSY-II at Open Circuit Potential (OCP) conditions and at OER-relevant potentials, above 1.62 V_{RHE}. Figure 1c shows the normalized data collected during chronoamperometry (CA) at 1.75 V_{RHE}, as well as at the OCP before and after the CA measurement.

The spectrum measured at OCP before the CA experiment reveals two Cu species, Cu^{I}_2O and $Cu^{II}(OH)_2/Cu^{II}O$, at 931.0 and 933.5 eV, respectively,[33−36] arising from the anodization synthesis of the electrocatalyst, as previously reported[26,37] and further confirmed by X-ray photoelectron spectroscopy (See Ex-situ characterization of the Cu-based electrocatalyst in the Supporting Information). Upon applied potential (1.75 V_{RHE}), the spectrum shows a new feature around 932.6 eV which lies between the Cu^{I} and Cu^{II} spectral features. Notably, this new feature disappears when returning to a relaxed state (OCP after CA. See Considerations about XAS at the OCP in the Supporting Information for more details about the relaxation behavior of the electrocatalyst). In fact, the spectrum recorded at the OCP after OER coincides with the data collected at the pristine OCP, prior to the CA at 1.75 V_{RHE}. The reversibility of the spectral feature emerging only under OER-relevant potentials suggests the formation of a metastable species or intermediate.

In order to speciate the complex appearing under the OER conditions and compare its fingerprint with those of the Cu-based species previously proposed as the key OER intermediate, it is worth inspecting the difference between the spectra at the OCP (pre-CA) and during the CA at the OER conditions as shown at the bottom of Figure 1c, providing more insights into the shape of the transient spectral feature. The spectral fingerprint of the new species, centered at 932.6 ± 0.2 eV, does not lie close to the L_3-edge energies associated with Cu^{II}, Cu^{I} (dashed lines in Figure 1c), or Cu^0 complexes (edge position similar to Cu^{I}),[27] suggesting that the new species possesses a different chemical environment. Comparison with reported organometallic and ternary complexes with formal Cu^{III} nature[38−41] reveals that the peak energy of the probed intermediate falls within the range of values observed for these complexes (930−935 eV, associated with the Lowest Unoccupied Molecular Orbital (LUMO)), suggesting that its electronic structure is more similar to these high-valent Cu species.

The reversible mechanism governing the appearance of this OER intermediate resembles the reaction previously reported in some Cu^{III}-hydroxide complexes.[42] In this context, "reversibility" refers to the consistent buildup of each chemical species before and after the OER conditions, as seen in Figure 1c, rather than the restoration of the catalyst to its original state, as copper dissolution occurs inevitably at high applied potentials. Severe dissolution of the electrocatalyst is observed under these conditions, as highlighted by the complete loss of Cu-associated spectroscopic signal at the electrode after the experiment depicted in the microspectrographs shown in Figure S8 of the Supporting Information.

Although the previous comparison with Cu L_3-edge energies reported in the literature points toward the formation of a high-valent Cu intermediate during OER, the wide range of Cu^{III} L_3-edge peak energies arising from the strong Cu 3d-ligand hybridization[38] (highlighting the ligand-driven nature of the LUMO) indicates the need for more detailed insights into the electronic structure of some Cu complexes. We can gain further understanding of the nature of these spectral features through *ab initio* calculations of projected density of states (pDOS) of Cu-based compounds with relevant oxidation states. Employing Density Functional Theory (DFT), the pDOSs of seven copper complexes were obtained as described in Materials and Experimental Methods in the Supporting Information, with their Cu d-states depicted in Figure 1d. As a good measure of the occupied and unoccupied states around the Fermi level, the Cu d-derived pDOS provides the basis for the spectral features probed experimentally. Specifically, the pDOS calculations include Cu^{I} and Cu^{II} complexes associated with the electrocatalyst's surface species in its relaxed state, like Cu^{I}_2O, $Cu^{II}(OH)_2$, and $Cu^{II}O$, as well as high-valent Cu complexes potentially related to the OER intermediate species, such as the ternary molecules $KCu^{III}O_2$, $LaCu^{III}O_2$, and $NaCu^{III}O_2$ or $Cu^{III}OOH$. By inspecting the unoccupied Cu d-states above the Fermi Energy (E_F), the presence of significant pDOS in $Cu^{II}(OH)_2$ and $Cu^{II}O$ around 0.5 eV can be associated with the spectral feature emerging around 931 eV in the *operando* Cu L_3-edge XAS in Figure 1c, attributed to the presence of Cu^{II} species at the surface of the electrocatalyst at OCP. Analogously, the pDOS contribution between 1.7 and 2.8 eV in Cu^{I}_2O relates to the Cu^{I} species in the pristine electrocatalyst.

Interestingly, the calculations of the high-valent Cu complexes reveal the emergence of unoccupied Cu d-states at energies between both species, around 0.5 eV < $E - E_F$ < 1.5 eV (Figure 1d), which can be related to the spectral feature associated with the OER intermediate probed under applied potential, at 932.6 eV. Specifically, the $KCu^{III}O_2$ and $NaCu^{III}O_2$ complexes exhibit the most significant pDOS contributions at this energy range, with a strongly localized state at 1.5 eV. Even considering the Cu s-derived states (shown exemplarily for $LaCu^{III}O_2$), only these two complexes depict abundant unoccupied electronic states in the energy region between the Cu^0/Cu^{I} and Cu^{II} fingerprints. This observation supports the association of the spectral feature attributed to the OER intermediate with high-valent copper species, similar to $KCu^{III}O_2$ and $NaCu^{III}O_2$. Likely, the new probed species presents an electronic structure similar to the $Cu^{III}O_2^-$ ion, present in both ternary complexes, as previously predicted.[16]

This combined experimental and theoretical analysis suggests that a high-valent copper species, likely similar to the $Cu^{III}O_2^-$ ion, participates in the oxygen evolution reaction mechanism with a 1.75 V_{RHE} applied potential. However, it is still unclear if this intermediate species appears exclusively at OER-relevant potentials (above the OER onset, defined as ∼1.7 V_{RHE} in this study) or if it emerges already at lower potentials, specifically in the redox region around 1.62 V_{RHE}. This question was addressed using a combination of Fixed-Energy X-ray Absorption Voltammetry (FEXRAV[43]) and Cyclic Voltammetry with varying upper potential limits (UPLs). With FEXRAV, the XAS signal at the photon energy associated with a distinct chemical species (the spectral fingerprint of the OER intermediate at 932, in this case) can

https://doi.org/10.1021/acs.jpclett.5c00944
J. Phys. Chem. Lett. 2025, 16, 6328−6333

be selectively monitored during potential-dependent measurements like Cyclic Voltammetry. Since the abundance of the chemical species in the electrocatalyst is proportional to the intensity of the collected spectroscopic signal, FEXRAV can shed light on the behavior of the monitored species and the dynamic processes dominating the electrochemical reaction.

The FEXRAV signal measured at 932.6 eV is shown in the top panel of Figure 2 while the bottom panel depicts the corresponding CVs. Collected for two different UPLs, the FEXRAV data reveal that the intermediate-related spectral fingerprint only appears for positive enough potentials, specifically, when the UPL is above the redox transition, coinciding with the potential regime where the OER occurs (see Figure S11 of the Supporting Information for more UPLs and scanning rates). When looking in more detail at the FEXRAV signal, it is evident that the spectroscopic intensity related to the new species, i.e., the abundance of the chemical species, grows for applied potentials above 1.62 V_{RHE} in the forward cycling direction (redox feature in the anodic branch, highlighted with a gray dashed line in Figure 2) and continues growing for higher potentials in the OER region until reaching a maximum at 1.55 V_{RHE} already in the backward direction (redox feature in the cathodic branch, gray dashed line), where the trend is reversed. At lower potentials in the reverse potential sweep, the abundance of this new species begins to decrease until its original concentration is reached around 1.0 V_{RHE}. The increase in the FEXRAV signal, which only occurs at the OER-related potential window between the anodic and cathodic features of this redox transition, suggests that the oxidation process and chemical transformation occurring at this redox potential are directly linked to the formation of the OER intermediate. Importantly, there is no evidence that the oxidative process at the redox feature produces a distinct product or intermediate compared with what is observed under the OER conditions. Instead, the results align with prior findings in this study, indicating that the OER intermediate likely corresponds to an oxidized species with a high-valent Cu nature.

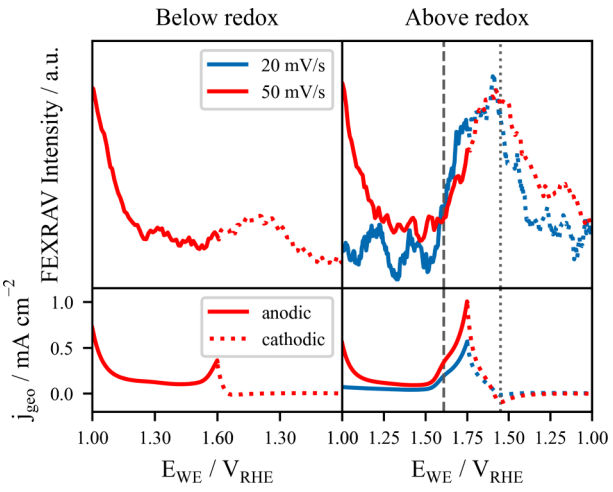

Figure 2. Potential-dependent study of the Cu-based electrocatalyst by FEXRAV at the characteristic excitation energy of the OER intermediate. (Top panel) FEXRAV signal at 932.6 eV, the spectral fingerprint of the intermediate species discussed above. Data is shown for two upper potential limits (UPLs): below (1.60 V_{RHE}, left panel) and above (1.75 V_{RHE}, right panel) the anodic redox feature. Also two scan rates are depicted: 20 mV/s (blue) and 50 mV/s (red). (Bottom panel) Corresponding CVs for the UPLs and scan rates mentioned, with the anodic branch (forward cycling direction) depicted as thick lines and the cathodic branch (backward potential sweep) as dashed lines. Gray dashed lines highlight the potentials of the redox couple in the anodic and cathodic branches.

To uncouple potentially undesired electrochemical reactions, FEXRAV measurements were performed at scan rates of 20 and 50 mV/s, as shown in Figure 2, with a slightly better signal quality due to the slower scanning (more points per mV). The 20 mV/s FEXRAV measurement shows a steep increase of the spectroscopic signal in the anodic branch around the anodic redox feature (~1.62 V_{RHE}). The smoother increase of the FEXRAV signal at 50 mV/s is due to the different scan rate, but the overall electrochemical behavior is independent of the scanning rate, indicating a system without diffusion-limited reactions (as further supported by the similarities between both CVs in the bottom panel of Figure 2).

In good agreement with the reversibility of the electrocatalyst observed with XAS before and after OER conditions, FEXRAV reveals that the original spectral fingerprint of the material is recovered in the backward potential sweep already at applied potentials below 1.3−1.4 V_{RHE} (depending on the scan rate), namely, below the cathodic part of the aforementioned redox couple. This finding further supports the relationship between the chemical transformations at the redox couple and the nature of the probed OER intermediate. While the FEXRAV analysis provides valuable insights into the redox and OER potential regions, it is important to note that a comprehensive understanding of the FEXRAV data for the full potential range shown in Figure 1b is beyond the scope of this work. The complete FEXRAV data set is provided in Figure S11 of the Supporting Information and involves multiple effects that are challenging to deconvolute at a single energy. These include potential Cu dissolution and the (dis)-appearance of specific Cu-containing species.

In conclusion, using *operando* Cu L_3-edge XAS, we probed the chemical species of the key intermediate governing alkaline OER in a Cu-based electrocatalyst. The electronic structure of this metastable species resembles that of high-valent Cu complexes, especially those associated with the CuO_2^- ion. The high-valent intermediate appears already at potentials as low as 1.62 V_{RHE}, coinciding with the oxidative reaction typically attributed to the $Cu^{2+} \leftrightarrow Cu^{3+}$ redox couple, while the original electrocatalyst state is recovered below 1.3−1.4 V_{RHE} depending on the scan rate of the cyclic voltammogram. This behavior suggests that the oxidative process at the redox potential is directly linked to the formation of the high-valent intermediate catalyzing the OER. Beyond the scope of the current work, further studies will explore the relationship between the probed OER intermediate, the limiting steps in the reaction's pathway, and the phenomenon of transpassive Cu dissolution.

■ ASSOCIATED CONTENT

Supporting Information

The Supporting Information is available free of charge at https://pubs.acs.org/doi/10.1021/acs.jpclett.5c00944.

The Supporting Information includes a Materials and Experimental Methods section and a section with further ex-situ characterization of the Cu-based electrocatalyst as well as more extended details about the computed

https://doi.org/10.1021/acs.jpclett.5c00944
J. Phys. Chem. Lett. 2025, 16, 6328−6333

pDOS of the 7 Cu-based compounds, about the XAS measurements at OCP and about the FEXRAV measurements with different UPLs and scanning rates (PDF)

Transparent Peer Review report available (PDF)

AUTHOR INFORMATION

Corresponding Author

Raul Garcia-Diez − *Interface Design, Helmholtz-Zentrum Berlin für Materialien und Energie GmbH (HZB), Berlin 12489, Germany;* orcid.org/0009-0000-9374-1083; Email: raul.garcia_diez@helmholtz-berlin.de

Authors

Romualdus Enggar Wibowo − *Interface Design, Helmholtz-Zentrum Berlin für Materialien und Energie GmbH (HZB), Berlin 12489, Germany;* Present Address: Young Investigator Group Electrochemical Conversion of CO2. Helmholtz-Zentrum Berlin für Materialien und Energie GmbH, Berlin 14109, Germany; orcid.org/0000-0002-8325-0413

Elmar Kataev − *Interface Design, Helmholtz-Zentrum Berlin für Materialien und Energie GmbH (HZB), Berlin 12489, Germany;* orcid.org/0000-0003-1016-946X

Wilson Quevedo Garzon − *Interface Design, Helmholtz-Zentrum Berlin für Materialien und Energie GmbH (HZB), Berlin 12489, Germany;* orcid.org/0000-0002-5222-6891

Marianne van der Merwe − *Interface Design, Helmholtz-Zentrum Berlin für Materialien und Energie GmbH (HZB), Berlin 12489, Germany;* orcid.org/0000-0002-3182-1392

Daniel Duarte-Ruiz − *Institute of Physics, Carl von Ossietzky Universität Oldenburg, Oldenburg 26129, Germany;* orcid.org/0000-0003-2424-1397

Caterina Cocchi − *Institute of Physics, Carl von Ossietzky Universität Oldenburg, Oldenburg 26129, Germany;* orcid.org/0000-0002-9243-9461

Marcus Bär − *Interface Design, Helmholtz-Zentrum Berlin für Materialien und Energie GmbH (HZB), Berlin 12489, Germany; Energy Materials In-Situ Laboratory Berlin (EMIL), HZB, Berlin 12489, Germany; Helmholtz Institute Erlangen-Nürnberg for Renewable Energy (HI ERN), Erlangen 91058, Germany; Dept. Chemistry and Pharmacy, Friedrich-Alexander-Universität Erlangen-Nürnberg, Erlangen 91058, Germany;* orcid.org/0000-0001-8581-0691

Complete contact information is available at: https://pubs.acs.org/10.1021/acs.jpclett.5c00944

Notes

The authors declare no competing financial interest.

ACKNOWLEDGMENTS

The authors would like to acknowledge Alexander Steigert (HZB) for the preparation by DC magnetron sputtering of the thin platinum current collector used in the electrocatalyst preparation, Mauricio D. Arce (CONICET) for fruitful discussion about electrochemical techniques, Anna Efimenko (HZB) and Mihaela Gorgoi (HZB) for the optimization of the EMIL beamline configuration and for beamtime support during the *operando* Cu L_3-edge XAS measurements, and Thomas Götsch (FHI) for support during the SEM measurements. RGD and MB are grateful for the financial support of the Bundesministerium für Bildung und Forschung (grant No. 03EW0015A/B), and MB and REW are grateful to the Deutsche Forschungsgemeinschaft (grant No. BA 2900/9-1). MB also acknowledges the Helmholtz Association, Impuls- und Vernetzungsfond for the grant No. VH-NG-423. CC and DDR acknowledge financial support from the German Federal Ministry for Education and Research (Professorinnenprogramm III). The authors are grateful to HZB for providing access to synchrotron radiation beamtime at BESSY II. Computational resources were provided by computing cluster ROSA at the University of Oldenburg, financed by the Lower Saxony Ministry of Science and Culture and by the German Research Foundation (Grant nr. INST 184/225-1 FUGG). The Energy Materials In-Situ Laboratory Berlin (EMIL) is acknowledged for providing the infrastructure for electrocatalyst preparation and off-synchrotron characterization (e.g., electrochemical and microscopic experiments).

REFERENCES

(1) Bernt, M.; Gasteiger, H. A. Influence of Ionomer Content in IrO2/TiO2 Electrodes on PEM Water Electrolyzer Performance. *J. Electrochem. Soc.* **2016**, *163*, F3179.

(2) Putra, R. P.; Horino, H.; Rzeznicka, I. I. An Efficient Electrocatalyst for Oxygen Evolution Reaction in Alkaline Solutions Derived from a Copper Chelate Polymer via In Situ Electrochemical Transformation. *Catalysts* **2020**, *10*, 233.

(3) Muthukumar, P.; Arunkumar, G.; Pannipara, M.; Al-Sehemi, A. G.; Moon, D.; Anthony, S. P. Highly enhanced electrocatalytic OER activity of water-coordinated copper complexes: effect of lattice water and bridging ligand. *RSC Adv.* **2023**, *13*, 12065−12071.

(4) Kumar, M. P.; Murugadoss, G.; Mangalaraja, R. V.; Kumar, M. R. Enhanced electrocatalytic activity of CuO-SnO2 nanocomposite in alkaline medium. *Appl. Phys. A: Mater. Sci. Process.* **2021**, *127*, 66.

(5) Huan, T. N.; Rousse, G.; Zanna, S.; Lucas, I. T.; Xu, X.; Menguy, N.; Mougel, V.; Fontecave, M. A Dendritic Nanostructured Copper Oxide Electrocatalyst for the Oxygen Evolution Reaction. *Angew. Chem., Int. Ed.* **2017**, *56*, 4792−4796.

(6) Gultom, N. S.; Abdullah, H.; Hsu, C.-N.; Kuo, D.-H. Activating nickel iron layer double hydroxide for alkaline hydrogen evolution reaction and overall water splitting by electrodepositing nickel hydroxide. *Chemical Engineering Journal* **2021**, *419*, 129608.

(7) Karthick, K.; Subhashini, S.; Kumar, R.; Sethuram Markandaraj, S.; Teepikha, M. M.; Kundu, S. Cubic Nanostructures of Nickel−Cobalt Carbonate Hydroxide Hydrate as a High-Performance Oxygen Evolution Reaction Electrocatalyst in Alkaline and Near-Neutral Media. *Inorg. Chem.* **2020**, *59*, 16690−16702.

(8) Bauer, D. J. et al. 2023 Critical Materials Strategy; 2023. DOI: 10.2172/1998242.

(9) Toparli, C.; Sarfraz, A.; Wieck, A. D.; Rohwerder, M.; Erbe, A. In situ and operando observation of surface oxides during oxygen evolution reaction on copper. *Electrochim. Acta* **2017**, *236*, 104−115.

(10) Guo, X.; Huang, H.; Liu, D. The inhibition mechanism and adsorption behavior of three purine derivatives on the corrosion of copper in alkaline artificial seawater: Structure and performance. *Colloids Surf., A* **2021**, *622*, 126644.

(11) Pan, L.; Han, Q.; Xie, X.; Xie, X.; Xiao, P. Corrosion Prevention of the Generator Stator Hollow Copper Conductor and Water Quality Adjustment of Its Internal Cooling Water. *Energy and Power Engineering* **2009**, *1*, 17−20.

(12) Ostervold, L.; Bakovic, S. I. P.; Hestekin, J.; Greenlee, L. F. Electrochemical biomass upgrading: degradation of glucose to lactic acid on a copper(ii) electrode. *RSC Adv.* **2021**, *11*, 31208−31218.

(13) Barragan, J. T. C.; Kogikoski, S. J.; da Silva, E. T. S. G.; Kubota, L. T. Insight into the Electro-Oxidation Mechanism of Glucose and

Other Carbohydrates by CuO-Based Electrodes. *Anal. Chem.* **2018**, *90*, 3357−3365.
(14) Müller, E. Über Passives Kupfer, Bezw. Das Anodische Verhalten des Kupfers in Natronlauge. *Zeitschrift für Elektrochemie und angewandte physikalische Chemie* **1907**, *13*, 133−145.
(15) Yue, Y.; Niu, J.; Yang, C.; Qin, J.; Zhang, X.; Liu, R. The OER/ORR activities of copper oxyhydroxide series electrocatalysts. *Molecular Catalysis* **2023**, *537*, 112942.
(16) Deng, Y.; Handoko, A. D.; Du, Y.; Xi, S.; Yeo, B. S. In Situ Raman Spectroscopy of Copper and Copper Oxide Surfaces during Electrochemical Oxygen Evolution Reaction: Identification of CuIII Oxides as Catalytically Active Species. *ACS Catal.* **2016**, *6*, 2473−2481.
(17) Ostervold, L.; Daneshpour, R.; Facchinei, M.; Tran, B.; Wetherington, M.; Alexopoulos, K.; Greenlee, L.; Janik, M. J. Identifying the Local Atomic Environment of the "Cu3+" State in Alkaline Electrochemical Systems. *ACS Appl. Mater. Interfaces* **2023**, *15*, 27878−27892.
(18) Deen, K. M.; Mehrjoo, N.; Asselin, E. Thermo−Kinetic diagrams: The Cu−H2O−Acetate and the Cu-H2O systems. *J. Electroanal. Chem.* **2021**, *895*, 115467.
(19) Celante, V. G.; Freitas, M. B. J. G. Electrodeposition of copper from spent Li-ion batteries by electrochemical quartz crystal microbalance and impedance spectroscopy techniques. *J. Appl. Electrochem.* **2010**, *40*, 233−239.
(20) Beverskog, B.; Puigdomenech, I. Revised Pourbaix Diagrams for Copper at 25 to 300°C. *J. Electrochem. Soc.* **1997**, *144*, 3476−3483.
(21) Gupta, N.; Segre, C.; Nickel, C.; Streb, C.; Gao, D.; Glusac, K. D. Catalytic Water Electrolysis by Co−Cu−W Mixed Metal Oxides: Insights from X-ray Absorption Spectroelectrochemistry. *ACS Appl. Mater. Interfaces* **2024**, *16*, 35793−35804.
(22) van der Merwe, M.; Lee, Y.; Wibowo, R. E.; Kokumai, T.; Efimenko, A.; Arce, M.; Jimenez, C. E.; Howchen, B.; Suarez Anzorena, R.; Lucentini, I.; Escudero, C.; Schuck, G.; Kochovski, Z.; Favaro, M.; Starr, D. E.; Reuter, K.; Scheurer, C.; Bär, M.; Garcia-Diez, R. Unravelling the mechanistic complexity of the oxygen evolution reaction and Ir dissolution in highly dimensional amorphous hydrous iridium oxides. *Energy Environ. Sci.* **2025**, *18*, 1214−1231.
(23) de Groot, F. M. F.; et al. 2p x-ray absorption spectroscopy of 3d transition metal systems. *J. Electron Spectrosc. Relat. Phenom.* **2021**, *249*, 147061.
(24) Velasco-Vélez, J.-J.; Skorupska, K.; Frei, E.; Huang, Y.-C.; Dong, C.-L.; Su, B.-J.; Hsu, C.-J.; Chou, H.-Y.; Chen, J.-M.; Strasser, P.; Schlögl, R.; Knop-Gericke, A.; Chuang, C.-H. The Electro-Deposition/Dissolution of CuSO4 Aqueous Electrolyte Investigated by In Situ Soft X-ray Absorption Spectroscopy. *J. Phys. Chem. B* **2018**, *122*, 780−787.
(25) Velasco-Vélez, J.-J.; Carbonio, E. A.; Chuang, C.-H.; Hsu, C.-J.; Lee, J.-F.; Arrigo, R.; Hävecker, M.; Wang, R.; Plodinec, M.; Wang, F. R.; Centeno, A.; Zurutuza, A.; Falling, L. J.; Mom, R. V.; Hofmann, S.; Schlögl, R.; Knop-Gericke, A.; Jones, T. E. Surface Electron-Hole Rich Species Active in the Electrocatalytic Water Oxidation. *J. Am. Chem. Soc.* **2021**, *143*, 12524−12534.
(26) Shu, X.; Zheng, H.; Xu, G.; Zhao, J.; Cui, L.; Cui, J.; Qin, Y.; Wang, Y.; Zhang, Y.; Wu, Y. The anodization synthesis of copper oxide nanosheet arrays and their photoelectrochemical properties. *Appl. Surf. Sci.* **2017**, *412*, 505−516.
(27) Garcia-Diez, R.; Frisch, J.; van der Merwe, M.; Wibowo, R. E.; Gorgoi, M.; Kataev, E.; Jimenez, C. E.; Arce, M. D.; Smith, W.; Quevedo-Garzon, W.; Wilks, R. G.; Wallacher, D.; Reinschlüssel, L. J.; Tok, G. C.; Gasteiger, H. A.; Bär, M. The OÆSE endstation at BESSY II: operando X-ray absorption spectroscopy for energy materials. *Journal of Synchrotron Radiation* **2025**, *32*, 634−648.
(28) Dong, S.; Xie, Y.; Cheng, G. Cyclic voltammetric and spectroelectrochemical studies of copper in alkaline solution. *Electrochim. Acta* **1992**, *37*, 17−22.
(29) Giri, S. D.; Sarkar, A. Electrochemical Study of Bulk and Monolayer Copper in Alkaline Solution. *J. Electrochem. Soc.* **2016**, *163*, H252.
(30) Ambrose, J.; Barradas, R. G.; Shoesmith, D. W. Investigations of copper in aqueous alkaline solutions by cyclic voltammetry. *Journal of Electroanalytical Chemistry and Interfacial Electrochemistry* **1973**, *47*, 47−64.
(31) Pyun, C.-H.; Park, S.-M. In Situ Spectroelectrochemical Studies on Anodic Oxidation of Copper in Alkaline Solution. *J. Electrochem. Soc.* **1986**, *133*, 2024.
(32) Abd el Haleem, S. M.; Ateya, B. G. Cyclic voltammetry of copper in sodium hydroxide solutions. *Journal of Electroanalytical Chemistry and Interfacial Electrochemistry* **1981**, *117*, 309−319.
(33) Zhang, X.; Zhou, J.; Song, H.; Chen, X.; Fedoseeva, Y. V.; Okotrub, A. V.; Bulusheva, L. G. "Butterfly Effect" in CuO/Graphene Composite Nanosheets: A Small Interfacial Adjustment Triggers Big Changes in Electronic Structure and Li-Ion Storage Performance. *ACS Appl. Mater. Interfaces* **2014**, *6*, 17236−17244.
(34) Saikova, S.; Vorobyev, S.; Likhatski, M.; Romanchenko, A.; Erenburg, S.; Trubina, S.; Mikhlin, Y. X-ray photoelectron, Cu L3MM Auger and X-ray absorption spectroscopic studies of Cu nanoparticles produced in aqueous solutions: The effect of sample preparation techniques. *Appl. Surf. Sci.* **2012**, *258*, 8214−8221.
(35) Sham, T. K.; Coulthard, I.; Lorimer, J. W.; Hiraya, A.; Watanabe, M. Reductive deposition of Cu on porous silicon from aqueous solutions: An X-ray absorption study at the Cu L3,2-edge. *Chem. Mater.* **1994**, *6*, 2085−2091.
(36) Chen, C. S.; Chen, T. C.; Chen, C. C.; Lai, Y. T.; You, J. H.; Chou, T. M.; Chen, C. H.; Lee, J.-F. Effect of Ti3+ on TiO2-Supported Cu Catalysts Used for CO Oxidation. *Langmuir* **2012**, *28*, 9996−10006.
(37) Meléndez-González, P. C.; Pech-Rodríguez, W. J.; Luévano-Hipólito, E.; Hernández-Ramírez, A.; Hernández-López, J. M. Innovative syntheses of immobilized CuxO semiconductors grown on 3D prints and their photoelectrochemical activity for sulfamethoxazole degradation. *Journal of Environmental Chemical Engineering* **2024**, *12*, 112551.
(38) DiMucci, I. M.; Lukens, J. T.; Chatterjee, S.; Carsch, K. M.; Titus, C. J.; Lee, S. J.; Nordlund, D.; Betley, T. A.; MacMillan, S. N.; Lancaster, K. M. The Myth of d8 Copper(III). *J. Am. Chem. Soc.* **2019**, *141*, 18508−18520.
(39) Huang, M.-J.; Deng, G.; Chin, Y. Y.; Hu, Z.; Cheng, J.-G.; Chou, F. C.; Conder, K.; Zhou, J.-S.; Pi, T.-W.; Goodenough, J. B.; Lin, H.-J.; Chen, C. T. Determination of hole distribution in $Sr_{14-x}Ca_xCu_{24}O_{41}$ using soft x-ray absorption spectroscopy at the Cu L_3 edge. *Phys. Rev. B* **2013**, *88*, 014520.
(40) Meyers, D.; Mukherjee, S.; Cheng, J.-G.; Middey, S.; Zhou, J.-S.; Goodenough, J. B.; Gray, B. A.; Freeland, J. W.; Saha-Dasgupta, T.; Chakhalian, J. Zhang-Rice physics and anomalous copper states in A-site ordered perovskites. *Sci. Rep.* **2013**, *3*, 1834.
(41) Choudhury, D.; Rivero, P.; Meyers, D.; Liu, X.; Cao, Y.; Middey, S.; Whitaker, M. J.; Barraza-Lopez, S.; Freeland, J. W.; Greenblatt, M.; Chakhalian, J. Anomalous charge and negative-charge-transfer insulating state in cuprate chain compound KCuO2. *Phys. Rev. B* **2015**, *92*, 201108.
(42) Dhar, D.; Yee, G. M.; Spaeth, A. D.; Boyce, D. W.; Zhang, H.; Dereli, B.; Cramer, C. J.; Tolman, W. B. Perturbing the Copper(III)−Hydroxide Unit through Ligand Structural Variation. *J. Am. Chem. Soc.* **2016**, *138*, 356−368.
(43) Minguzzi, A.; Lugaresi, O.; Locatelli, C.; Rondinini, S.; D'Acapito, F.; Achilli, E.; Ghigna, P. Fixed energy X-ray absorption voltammetry. *Anal. Chem.* **2013**, *85*, 7009−7013.

https://doi.org/10.1021/acs.jpclett.5c00944
J. Phys. Chem. Lett. 2025, 16, 6328−6333